Scattering of hot excitons due to optical phonons in quantum wells: Multiphonon resonant Raman process

C. Trallero-Giner,[1] Fernando de León-Pérez,[1,2] Meng Lu,[3] and Joseph L. Birman[3]
[1]*Department of Theoretical Physics, Havana University, 10400 Havana, Cuba*
[2]*Physics Department, Central University "Marta Abreu" of Las Villas, Santa Clara, Cuba*
[3]*Department of Physics, The City College of CUNY, New York, New York, 10031*
(Received 8 October 2001; published 22 February 2002)

The hot-exciton scattering rate by optical phonons is calculated in the framework of the envelope-function approximation in narrow quantum wells (QWs). The exciton-phonon Fröhlich-type interaction is considered and the contributions of the confined phonons and interface modes to the total scattering rate are discussed in terms of the in-plane exciton kinetic energy and quantum-well width. To take into account the full symmetry of the optical phonons a phenomenological approach is employed in which the mechanical and electrostatic matching boundary conditions are fulfilled at QW interfaces. It is shown that the main contribution to the scattering rate comes from intrasubband transition assisted by phonons with even electrostatic potential state. The experimental observation in short period GaAs/AlAs superlattices on the phonon symmetries and their relative intensities of multiphonon resonant Raman process is qualitatively explained in terms of the relative role of the confined and interface optical phonons on the exciton scattering rate.

DOI: 10.1103/PhysRevB.65.115314 PACS number(s): 63.20.Kr, 71.35.−y, 78.66.−w

I. INTRODUCTION

An exciton with kinetic energy higher than the thermal temperature of the medium is called a hot exciton. This concept has been introduced in the past when multiphonon LO lines have been observed in resonant Raman scattering in bulk semiconductor materials (see Ref. 1 and references therein). For polar semiconductors, when the exciton energy is greater than a longitudinal optical phonon, the scattering rate is governed by the Fröhlichlike mechanism playing the main role in the intraband exciton relaxation time. In the past and for the bulk semiconductor case, transition probabilities of hot excitons interacting with longitudinal and acoustic phonons have been carried out in Refs. 2–4. The dependence on exciton kinetic energy, effective electron and hole masses, and on the excitonic quantum numbers were obtained, showing the conditions that favored the hot-exciton contribution to the multiphonon Raman process in semiconductors.

The importance of hot-exciton relaxation via optical-phonon emission in quantum wells (QWs) has been stressed by photoluminescence experiments[5,6] and by time-resolved Raman scattering measurements.[6,7] Also, the relative role of confined phonons and interface modes in time-resolved resonant Raman spectroscopy experiments is pointed out in Ref. 8. Today, there are several theoretical studies of carrier relaxation times in QWs considering the main mechanism due to electron-LO-phonon interaction (e.g., Ref. 9 and references therein). In Refs. 10–12 the exciton linewidths in quantum-well structures due to bulk LO phonons have been obtained considering different approach for the excitonic states. Calculations taking into account scattering to higher subbands and to the continuum excitonic states as a function of the QW width are reported in Refs. 12 and 13.

In this paper, we will focus on the hot-exciton scattering-rate calculation due to the confined phonons and interface optical modes and their contribution to the multiphonon resonant Raman process (MPR) in narrow QWs. Hot-exciton relaxation and resonant Raman scattering due to combination of bulk LO phonons have been measured in GaAs/AlGaAs multiple QWs by Clèrot *et al.*[14] In Ref. 15, Mowbray *et al.* reported multiphonon processes in short-period GaAs/ AlAs superlattices at laser energies above the type-I band gap. The corresponding Raman spectra for the second- and third-order processes from GaAs phonons show structures involving the combination of confined and interface optical modes. Their relative intensities do not follow the expected products of the observed first-order Raman intensity. As it is shown in Fig. 1(a) for the case of third-order process of 10-GaAs monolayer samples, the combined intensities of LO_2 and LO_4 phonons are comparable to the intensities due to $3LO_2$ one. The relative intensities of the second- (not shown) and third-order processes due to the combination of LO_2-confined phonon are weaker than that obtained with LO_2 and interface phonons as it is observed in Fig. 1(b) for the 6 GaAs monolayer. These results show that the relative intensities of the MPR scattering process are very sensitive to the quantum well width. We need to emphasize that the reported MPR processes correspond to the scattering light coming from the direct gap of the GaAs, that is, the exciton relaxation observed in the Raman spectra of Fig. 1 comes from the Γ point of the Brillouin zone.

The connection between the MPR process with excitonic transitions follows when the excitonic cascade model is invoked to explain the main features of the scattered light.[14,16] According to this model, the Raman intensity $I^{(N)}$ of a Nth-order ($N=n_1+\cdots+n_N$) phonon process is proportional to the indirect exciton creation probability, $F_{\alpha}^{(n_1)}$, by the light after the emission of one L_{n_1} phonon, to the exciton cascade scattering probabilities, $W^{(n_i)}_{\alpha_i\to\alpha_{i+1}}$, with emission of $n_2+\cdots+n_{N-1}$ phonons, and finally to the indirect annihilation probability $\Lambda^{(n_N)}_{\alpha_N}$ assisted by L_{n_N} phonon. That is,

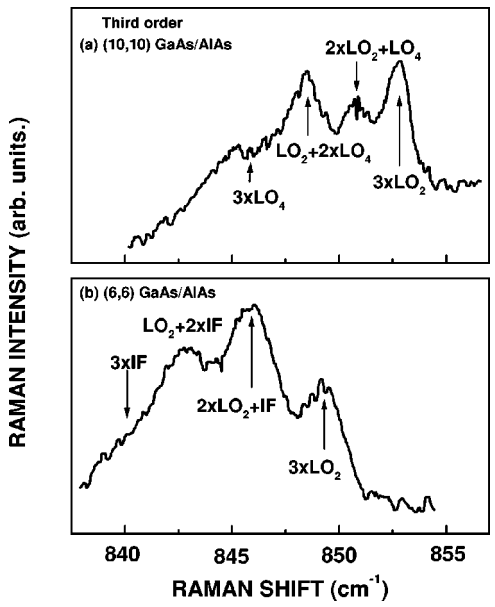

FIG. 1. Third-order Raman GaAs phonon spectra from Ref. 15. (a) (10,10) and (b) (6,6) [GaAs, AlAs] monolayers. Arrows indicate the position of overtones and combinations of confined LO phonons and interface modes.

$$I^{(n_1+n_2+\cdots+n_N)}\sim F_{\alpha}^{(n_1)}\left(\prod_{i=1}^{N-2}\frac{W_{\alpha_i\rightarrow\alpha_{i+1}}^{(n_i)}}{W_{\alpha i}}\right)\Lambda_{\alpha_N}^{(n_N)}. \tag{1}$$

Here, the excitonic state is labeled by α and the phonon symmetry by n_i, and $(W_{\alpha_i})^{-1}$ is the total-exciton lifetime in the state α which it is mainly determined by the Γ-X excitonic transition (the GaAs/AlAs QW has an indirect gap in the X point). According to Eq. (1), an explicit calculation of $W_{\alpha\rightarrow\alpha'}^{(n)}(E_K)$ as a function of the QW width, exciton kinetic energy E_K, and phonon mode L_n will bring a further understanding of MPR process in QWs as we will discuss below.

II. MODEL AND FUNDAMENTAL EXPRESSIONS

To describe the scattering-rate process we assume a Wannier-Mott exciton model in a quantum well with nondegenerate electron and hole isotropic bands. In the framework of the envelope-function approximation, for narrow quantum wells and in the adiabatic approximation, where the three-dimensional excitonic Bohr radius a_B is larger than the electron-hole pair mean value along the growth direction, the eigenvalues and eigenfunctions of the quantum-confined excitons are described by the Hamiltonian

$$H(\mathbf{r}_e,\mathbf{r}_h)=H_0(\mathbf{r}_e,\mathbf{r}_h)+H_p(\mathbf{r}_e,\mathbf{r}_h), \tag{2}$$

with

$$H_0=p_e\left(\frac{1}{2m_e(z_e)}p_e\right)+p_h\left(\frac{1}{2m_h(z_h)}p_h\right)-\frac{e^2}{\epsilon\rho}+V_e(z_e)+V_h(z_h), \tag{3}$$

and H_p is considered as a perturbation to the Hamiltonian (3) given by

$$H_p=-\frac{e^2}{\epsilon}\{[(\boldsymbol{\rho}_e-\boldsymbol{\rho}_h)^2+(z_e-z_h)^2]^{-1/2}-|\boldsymbol{\rho}_e-\boldsymbol{\rho}_h|^{-1}\}, \tag{4}$$

where ϵ is the dielectric constant, $m_e(m_h)$, $\mathbf{r}_e=(\boldsymbol{\rho}_e,z_e)$ $[\mathbf{r}_h=(\boldsymbol{\rho}_h,z_h)]$, and $V_e(z_e)$ $[V_h(z_h)]$ are the effective mass, the coordinates, and band offset for the electron (hole), respectively. The exciton wave function $\Psi_{exc}(\mathbf{r}_e,\mathbf{r}_h)$ of the Hamiltonian H_0 can be taken in separable form given by products of the two-dimensional exciton wave function $\Psi(\mathbf{R},\boldsymbol{\rho})$ and the electron and hole subband wave functions $\phi_i(z_i)$ $(i=e,h)$

$$\Psi_{exc}(\mathbf{r}_e,\mathbf{r}_h)=\Psi(\mathbf{R},\boldsymbol{\rho})\phi_e(z_e)\phi_h(z_h). \tag{5}$$

The exciton in-plane motion is described by the electron-hole pair center-of-mass coordinate $\mathbf{R}=(m_e\boldsymbol{\rho}_e+m_\perp^h\boldsymbol{\rho}_h)/M$ $(M=m_e+m_\perp^h)$ and the in-plane relative coordinate of the electron and the hole $\boldsymbol{\rho}=\boldsymbol{\rho}_e-\boldsymbol{\rho}_h$. The wave functions $\phi(z)$ and eigenenergies E_n are given elsewhere.[17] The two-dimensional exciton wave function in polar coordinates can be separated into a center of mass motion with wave vector $\mathbf{K}$, a radial part, and an angular part given by

$$\Psi(\mathbf{R},\boldsymbol{\rho})=\frac{1}{\sqrt{S}}e^{i\mathbf{K}\cdot\mathbf{R}}R_{N,m}(\rho)\frac{1}{\sqrt{2\pi}}e^{im\theta},\quad m=0,\pm1,\pm2,\ldots, \tag{6}$$

and S is the QW area. For bound exciton states the corresponding normalized eigenfunctions are obtained as follows:[18]

$$R_{N,m}(\rho)=N_{N,m}e^{-\rho/[a_B(N+1/2)]}\left[\frac{2\rho}{a_B(N+1/2)}\right]^{|m|}\times F\left[-N+|m|,2|m|+1,\frac{2\rho}{a_B(N+1/2)}\right];\quad |m|\leqslant N, N=0,1,\ldots, \tag{7}$$

where

$$N_{N,m}=\sqrt{\frac{(N+|m|)!}{[(2m)!]^2a_B^2(N+1/2)^3(N-|m|)!\,\pi}}, \tag{8}$$

$F(\alpha,\beta;z)$ is the confluent hypergeometric function, and the bound exciton energies ε_N are

$$\varepsilon_N=-\frac{R_y}{(N+1/2)^2},\quad N=0,1,\ldots. \tag{9}$$

The total energy of Hamiltonian (2) is found to be

$$E=E_g+E_{n_e}+E_{n_h}+\varepsilon_N+\Delta E_{N,m}^{n_e,n_h}+\frac{\hbar^2K^2}{2M}, \tag{10}$$

with E_g being the gap energy, $\Delta E_{N,m}^{n_e,n_h}$ is the three-dimensional Coulomb correction, $R_y=\mu e^2/2\hbar^2\epsilon^2$ is the ef-

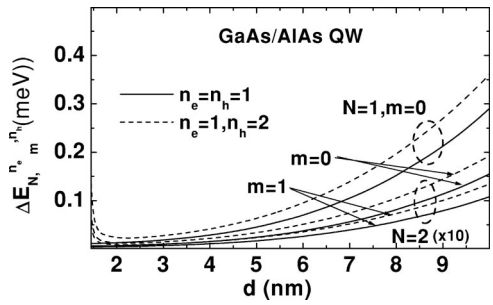

FIG. 2. Excitonic correction $\Delta E^{n_e,n_h}_{N,m}$ given by Eq. (11) for the $n_e=n_h=1$ (solid lines) and $n_e=1,n_h=2$ (dashed lines) excitonic branches in GaAs/AlAs QW as a function of the width d. The $N=1$ and $N=2$ ($m=0,1$) internal excitonic states are considered.

fective Rydberg constant, and μ the reduced mass in the XY plane. The $\Delta E^{n_e,n_h}_{N,m}$ value as function of QW width can be found from the Hamiltonian (4) in first-order perturbation theory. In the adiabatic approximation, where the Z-axis confinement is stronger than for the XY direction, i.e., if the Bohr radius is larger than the QW width, the electron-hole mean value in the XY plane is bigger than the electron-hole pair mean separation along the Z-axis and the excitonic correction can be approximately given by

$$\Delta E^{n_e,n_h}_{N,m}=\langle N,m;n_e,n_h|H_p|n_h,n_e;m,N\rangle \equiv -\frac{e^2}{2\epsilon r^3_{N,m}}[\langle n_e|z_e^2|n_e\rangle+\langle n_h|z_h^2|n_h\rangle\cdots], \quad (11)$$

where the mean electron-hole separation $r_{N,m}=\langle N,m|r|m,N\rangle$ can be cast as

$$r_{N,m}=a_B\sqrt{\frac{(N+1/2)(N+|m|)!\Gamma(\gamma+3)N!}{(2m)!(N-|m|)!(\gamma+N-1)!\pi}}\times\sqrt{\left[1+12\frac{N}{\gamma}+30\frac{N(N-1)}{\gamma(\gamma+1)}+20\frac{N(N-1)(N-2)}{\gamma(\gamma+1)(\gamma+2)}\right]}, \quad (12)$$

$\gamma=2|m|+1$, $\Gamma(x)$ represents the Gamma function, and the functions $\langle n|z^2|n\rangle$ are reported in Ref. 18. The numerical results for the three-dimensional (3D) excitonic correction $\Delta E^{n_e,n_h}_{N,m}$ in GaAs/AlAs QW are shown in Fig. 2 as a function of the quantum well width d. The first two excitonic branches ($n_e=1$, $n_h=1$ and $n_e=1$, $n_h=2$) and different internal quantum numbers N,m are considered. As can be seen in the figure, the 3D exciton corrections decrease as d decreases causing the exciton to become more 2D. For the QW width d smaller than a certain value d_0, the $\Delta E^{n_e,n_h}_{N,m}$ correction grows rapidly because the carrier becomes less confined and the adiabatic approximation is not longer valid. In the case of GaAs/AlAs QW, the lower value of d for which the excitonic branch $n_e=1$, $n_h=2$ exist corresponds to $d=1.4$ nm. Moreover, the excitonic correction given by Eq. (11) is sustained under the approximation $\langle N,m|(z_e^2+z_h^2)|m,N\rangle<r^2_{N,m}$ and our calculations have been limited to $d\geqslant 1.4$ nm. As can be seen in Fig. 2, the contribution of $\Delta E^{n_e,n_h}_{N,m}$ to the exciton energy ε_N is very small in the range 1.6 nm$<d<7$ nm an in principle can be disregarded.

To describe the exciton-phonon interaction we follow a unified treatment that takes into account the full matching boundary conditions: mechanical and electrodynamic.[19] This phenomenological treatment involves the coupling between the longitudinal (L) and transversal (T) polarization modes as a consequence of the coupled differential equations for the phonon-displacement field $\mathbf{u}$ and electrostatic potential φ. This model, particularly useful to describe Raman process,[20–22] yields confined quasi-L and confined quasi-T modes, while some of these modes exhibit interface character. The interaction Hamiltonian is[19]

$$H_{E-P}=\sum_{n_p,\mathbf{q}}\frac{C_F}{\sqrt{V}}[\varphi_{n_p,\mathbf{q}}(z_e)e^{i\mathbf{q}\cdot\boldsymbol{\rho}_e}-\varphi_{n_p,\mathbf{q}}(z_h)e^{i\mathbf{q}\cdot\boldsymbol{\rho}_h}]\times\hat{b}_{n_p,\mathbf{q}}+\text{H.c.}, \quad (13)$$

where $\hat{b}_{n_p,\mathbf{q}}$ is the phonon creation operator with wave vector $\mathbf{q}$ and frequency $\omega_{n_p,q}$. $V=Sd$ is a normalization volume, and C_F is the Fröhlich coupling constant given by

$$C_F=e\sqrt{2\pi\hbar\omega_L(\epsilon_\infty^{-1}-\epsilon_0^{-1})}, \quad (14)$$

where ω_L is the LO phonon frequency, ϵ_∞ is the high-frequency dielectric constant, and ϵ_0 is the static dielectric constant. The Fröhlich-type exciton-phonon interaction (13) has been expressed as a product of factors for motion perpendicular and parallel to the QW axis. The function $\varphi_{n_p,\mathbf{q}}$ is proportional to the electrostatic scalar potential obtained as solution of the eigenvalue problem and shows a definite parity. We need to remark that the potential given in Refs. 19,23 has several misprints. The correct expressions are written below.

(A) Odd-potential states

$$\varphi_{n_p,\mathbf{q}}(z)=\sqrt{\frac{d}{\|u\|^2}}\begin{cases}\sin(2\eta_L z/d)-S_L^+e^{-\eta_q}\sinh(2\eta_q z/d)/\eta_q, & |z|\leqslant d/2,\\ S_0e^{-2\eta_q|z|/d}z/|z|, & |z|\geqslant d/2,\end{cases} \quad (15)$$

with the following dispersion relation:

$$\left(\frac{\beta_L}{\beta_T}\right)^2[\eta_L^2+\eta_q^2](\eta_L\cos\eta_L+\eta_q\sin\eta_L)\times(\eta_q\cos\eta_T\sinh\eta_q+\eta_T\sin\eta_T\cosh\eta_q)=[\eta_T^2+\eta_q^2](\eta_q\cos\eta_T-\eta_T\sin\eta_T)\times(\eta_L\cos\eta_L\sinh\eta_q-\eta_q\sin\eta_L\cosh\eta_q), \quad (16)$$

where β_L and β_T are two parameters describing the quadratic dispersion of the L and T phonons in the bulk, respectively.

(B) Even-potential state

$$\varphi_{n_p,\mathbf{q}}(z)=\sqrt{\frac{d}{||u||^2}}\begin{cases}\cos(2\eta_L z/d)-C_L^+ e^{-\eta_q} & \\ \quad\times\cosh(2\eta_q z/d)/\eta_q, & |z|\leqslant d/2,\\ C_0 e^{-2\eta_q|z|/d}, & |z|\geqslant d/2,\end{cases} \tag{17}$$

with the following dispersion relation:

$$\begin{aligned}\left(\frac{\beta_L}{\beta_T}\right)^2[\eta_L^2+\eta_q^2](\eta_q\cos\eta_L-\eta_L\sin\eta_L)&\\ \times(\eta_T\cos\eta_T\sinh\eta_q-\eta_q\sin\eta_T\cosh\eta_q)&\\ =[\eta_T^2+\eta_q^2](\eta_T\cos\eta_T+\eta_q\sin\eta_T)&\\ \times(\eta_L\sin\eta_L\cosh\eta_q+\eta_q\cos\eta_L\sinh\eta_q).&\end{aligned} \tag{18}$$

In Eq. (15) and Eq. (17), $\|u\|^2$ represents the norm of the vibrational amplitude. The definition of the terms S_L^+, C_L^+, $\|u\|^2$, and other parameters can be found in the Appendix.

The sinusoidal and cosenusoidal functions appearing in Eq. (15) and Eq. (17), respectively, are the contributions of the confined phonons to the electrostatic potential, while the hyperbolic and exponential functions come from the interface phonons and are due to the dielectric mismatch between the interfaces. It is important to realize that the modes may be predominantly *L*, or predominantly *T*, or present certain character of ''interface'' modes, depending on wave vector **q**, which is contained in Eq. (16) and Eq. (18).

The phonon dispersions for a structure of GaAs/AlAs with 2.8, 2.0, and 1.7 nm well width are shown in Fig. 3. The branches are labeled as L_{n_p} and T_{n_p} ($n_p=1,2,3,\ldots$) according to their longitudinal and transverse character at $\mathbf{q}=0$. The modes that show a strong dispersion as a function of the in-plane wave vector **q** are those with the strongest electric-field component and also the strongest interface character. For the 2.8 nm and 1.7 nm QW width the two interface branches are L_1 and T_1 modes, while in the case of Fig. 3(b) these correspond to L_1 and L_4 modes. The upper mode is purely antisymmetric (L_1) while the lower interface mode (T_1 and L_4 in Fig. 3) is symmetric. As $\mathbf{q}\neq 0$, the upper (lower) interface phonon has solely contribution from antisymmetric (symmetric) modes. In the figure anticrossings can be observed between those states with the same symmetry. These anticrossings of the confined and interface phonons have been observed in GaAs/AlAs multiple QWs, where the interface roughness scattering induces the necessary phonon wave vector.[21]

III. SCATTERING RATE

The scattering probability per unit time of an exciton in a QW from the initial **K**, *N*, *m*; n_e, n_h to final $\mathbf{K}'$, N', m'; n_e', n_h' states due to the interaction with optic phonon is given by

$$\begin{aligned}W^{(n_p)}_{N,m;n_e,n_h\to N',m';n_e',n_h'}(\mathbf{K},\mathbf{K}')&\\ =\frac{2\pi}{\hbar}\sum_{\mathbf{q}}|\langle\mathbf{K},N,m;n_e,n_h|H_{E-P}|n_h',n_e';m',N',\mathbf{K}'\rangle|^2&\\ \times\delta\left(\frac{\hbar^2K'^2}{2M}-\frac{\hbar^2K^2}{2M}+\hbar\omega_{n_p,q}+E_{n_e'}-E_{n_e}+E_{n_h'}-E_{n_h}\right.&\\ \left.+\varepsilon_{N'}-\varepsilon_N+\Delta E^{n_e',n_h'}_{N',m'}-\Delta E^{n_e,n_h}_{N,m}\right).&\end{aligned} \tag{19}$$

We consider the case of low temperature where $k_BT\ll\hbar\omega_{n_p,q}$ (k_B is the Boltzmann constant) and the phonon emission Stokes process is the main process. It is clear that obtaining scattering probability considering the phonon-absorption process is straightforward if the phonon occupation number $N(\mathbf{q})=[e^{\hbar\omega_{n_p,\mathbf{q}}/k_BT}-1]^{-1}$ is introduced on the right-hand side (rhs) of Eq. (19) and $\hbar\omega_{n_p,\mathbf{q}}$ is substituted by $-\hbar\omega_{n_p,\mathbf{q}}$. In the adiabatic approximation the wave function Eq. (5) and the exciton-phonon Hamiltonian (13) permit us to write the matrix element in Eq. (19) as

$$\begin{aligned}\langle\mathbf{K},N,m;n_e,n_h|H_{E-P}|n_h',n_e';m',N',\mathbf{K}'\rangle&\\ =\frac{C_F}{\sqrt{V}}\delta_{\mathbf{K}',\mathbf{K}-\mathbf{q}}[I^{N',m'}_{N,m}(Q_h)\langle n_e|\varphi_{n_p,\mathbf{q}}|n_e'\rangle\delta_{n_h,n_h'}&\\ -I^{N',m'}_{N,m}(Q_e)^*\langle n_h|\varphi_{n_p,\mathbf{q}}|n_h'\rangle\delta_{n_e,n_e'}],&\end{aligned} \tag{20}$$

where $Q_{h(e)}=m^h_\perp(m_e)a_Bq/M$. The first (second) term in the rhs of Eq. (20) is due to the phonon emission by the electron (hole) with matrix elements $I^{N',m'}_{N,m}(Q_h)[I^{N',m'}_{N,m}(Q_e)]$ in the *XY* plane and $\langle n_e|\varphi_{n_p,\mathbf{q}}|n_e'\rangle(\langle n_h|\varphi_{n_p,\mathbf{q}}|n_h'\rangle)$ along the *Z* axis. The transition-matrix elements $I^{N',m'}_{N,m}$ are given in the Appendix. Substituting Eq. (20) into Eq. (19) and carrying out the sum over $\mathbf{K}'$ one can find the scattering rate as a function of the absolute value of the exciton wave vector **K**

$$\begin{aligned}W^{(n_p)}_{N,m;n_e,n_h\to N',m';n_e',n_h'}&\\ =\frac{C_F^2}{2\pi\hbar d}\int_0^\infty dqq\int_0^{2\pi}d\theta_1|I^{N',m'}_{N,m}(Q_h)&\\ \times\langle n_e|\varphi_{n_p,\mathbf{q}}|n_e'\rangle\delta_{n_h,n_h'}&\\ -I^{N',m'}_{N,m}(Q_e)^*\langle n_h|\varphi_{n_p,\mathbf{q}}|n_h'\rangle\delta_{n_e,n_e'}|^2\delta(f(q,\theta_1)),&\end{aligned} \tag{21}$$

where

$$\begin{aligned}f(q,\theta_1)=\frac{\hbar^2q^2}{2M}-\frac{\hbar^2Kq}{M}\cos\theta_1+\hbar\omega_{n_p,q}+E_{n_e'}-E_{n_e}+E_{n_h'}&\\ -E_{n_h}+\varepsilon_{N'}-\varepsilon_N+\Delta E^{n_e',n_h'}_{N',m'}-\Delta E^{n_e,n_h}_{N,m},&\end{aligned} \tag{22}$$

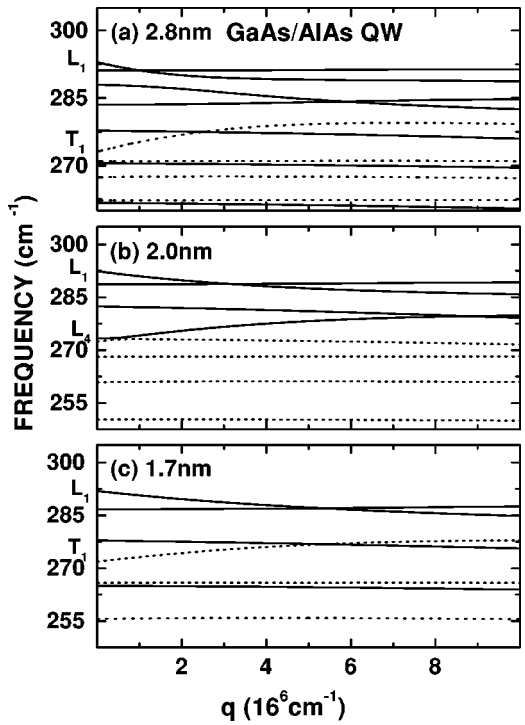

FIG. 3. Dispersion of the GaAs optical phonons of the (a) 2.8 nm, (b) 2.0 nm, and (c) 1.7 nm GaAs/AlAs quantum well. The phonons are labeled as longitudinal (L) and transverse (T) according to its character at $\mathbf{q}=0$. Interface phonon branches are those showing strong dispersion as a function of $\mathbf{q}$ and are indicted by L_1, L_4, and T_1 in (a), (b), and (c), respectively. The anticrossing of L_4 and T_1 modes near $\mathbf{q}=5\times10^5$ cm^{-1} is clearly seen in (b). L_4 and T_1 modes present the same parity respect to center of the QW.

and θ_1 is the angle between vectors $\mathbf{K}$ and $\mathbf{q}$. The energy and momentum conservation laws restrict the absolute value of the phonon wave vector $\mathbf{q}$ within the range of q_{min} and q_{max}, which are solutions of

$$f_{\pm}(E_K)\equiv q_0^2 \pm 2\sqrt{\frac{M}{\mu}}\sqrt{\frac{E_K}{R_y}}q_0+\frac{M}{\mu R_y}(\hbar\omega_{n_p,q}+E_{n_e'}-E_{n_e}+E_{n_h'}-E_{n_h}+\varepsilon_{N'}-\varepsilon_N)=0, \tag{23}$$

with the condition $q_{min}\geqslant 0$, $q_0=qa_B$, and $E_K=\hbar^2K^2/2M$ is the exciton kinetic energy. After the integration with respect to θ_1 and summation over m and m' in Eq. (21), we obtain

$$W^{(n_p)}_{N;n_e,n_h\to N';n_e',n_h'}(E_K) = 2\omega_L\frac{M}{a_B\mu d}\left(\frac{\epsilon_0}{\epsilon_\infty}-1\right)\int_{q_{min}}^{q_{max}}\frac{dq_0q_0}{\sqrt{f_+(E_K)f_-(E_K)}} \times\sum_{m,m'}|e^{i(m'-m)\theta_1}I^{N',m'}_{N,m}(Q_h)\langle n_e|\varphi_{n_p,\mathbf{q}}|n_e'\rangle\delta_{n_h,n_h'} - e^{-i(m'-m)\theta_1}I^{N',m'}_{N,m}(Q_e)^*\langle n_h|\varphi_{n_p,\mathbf{q}}|n_h'\rangle\delta_{n_e,n_e'}|^2, \tag{24}$$

with θ_1 is given by

$$\tan\theta_1(E_K)=2\frac{\sqrt{f_+(E_K)f_-(E_K)}}{f_+(E_K)+f_-(E_K)}. \tag{25}$$

From the energy and quasimomentum conservation laws it follows that the scattering probability $W^{(n_p)}$ is different from zero if the exciton kinetic energy $E_K>\hbar\omega_{n_p,q}+E_{n_e'}-E_{n_e}+E_{n_h'}-E_{n_h}+\varepsilon_{N'}-\varepsilon_N+\Delta E^{n_e',n_h'}_{N',m'}-\Delta E^{n_e,n_h}_{N,m}$. In Fig. 4, we illustrate the content of Eq. (24), showing the types of one-phonon Stokes scattering processes included in the scattering rate. Each exciton band is characterized by single electron and hole quantum numbers (n_e,n_h) and the total quantum number N: two excitonic bands are shown including dispersion due to center-of-mass motion as in Eq. (10). For an exciton excited to the initial state labeled A in the Fig. 4, and in the adiabatic approximation used here, only two processes will occur: (a) intrasubband scattering, with phonon potential state of even parity ($n_p=2,4,\ldots$) and $n_e=n_e'=1$ and $n_h=n_h'=1$; (b) inter-intrasubband scattering (mixed process) given by $n_e=n_e'=1$ but $n_h\neq n_h'$ and vice versa. Here, if $|n_h-n_h'|$ is even the phonon potential is an even function, while for $|n_h-n_h'|$ equal to an odd number, the phonon potential states need to be odd giving a zero electron contribution to the scattering probability. This is illustrated in Fig. 4, where single-phonon inter-intrasubband scattering are shown by arrows $A\to B$, $A\to C$, defining the corresponding q_{min} and q_{max} for these processes. The exciton intrasubband transitions ($A\to B'$,$A\to C'$) are coupled to the symmetric part of the phonon potential, while the exciton intersubband scattering (with mixed character or not) couples to the symmetric or antisymmetric part of the Fröhlich Hamiltonian interaction. All such inter and intrasubband processes need to be included, taking account also of the restrictions on allowed pairs (n_e,n_h), (n_e',n_h') due to conservation of energy and quasimomentum that is included in Eq. (24). The total exciton scattering rate characterized by the quantum number $N=0$; $n_e=1$, $n_h=1$ and kinetic energy E_k and due to the interaction with an optical phonon n_p can be written as

$$W^{(n_p)}_{0;1,1}(E_K)=W^{(n_p)}_{0;1,1\to 0;1,1}(E_K)+\sum_{N'\neq 0}W^{(n_p)}_{0;1,1\to N';1,1}(E_K) + \sum_{N'\neq 0}^{n_e\neq n_e' \text{ or } n_h\neq n_h'} W^{(n_p)}_{0;1,1\to N';n_e',n_h'}(E_K). \tag{26}$$

The first term on the rhs of the above Eq. (26) represents the intraband scattering probability without changes of the internal state $N=0$ of the exciton band $n_e=1$, $n_h=1$. The second term is the exciton intraband scattering accompanied by transitions from $N=0$ to other internal quantum states $N'\neq 0$, while the last term gives the intersubband contribution to the exciton lifetime in the branch $n_e=1$,$n_h=1$ with internal quantum number $N=0$ and kinetic energy E_K. In the next section, we study the dependence of the scattering rate on the in-plane kinetic energy, and on the phonon state n_p.

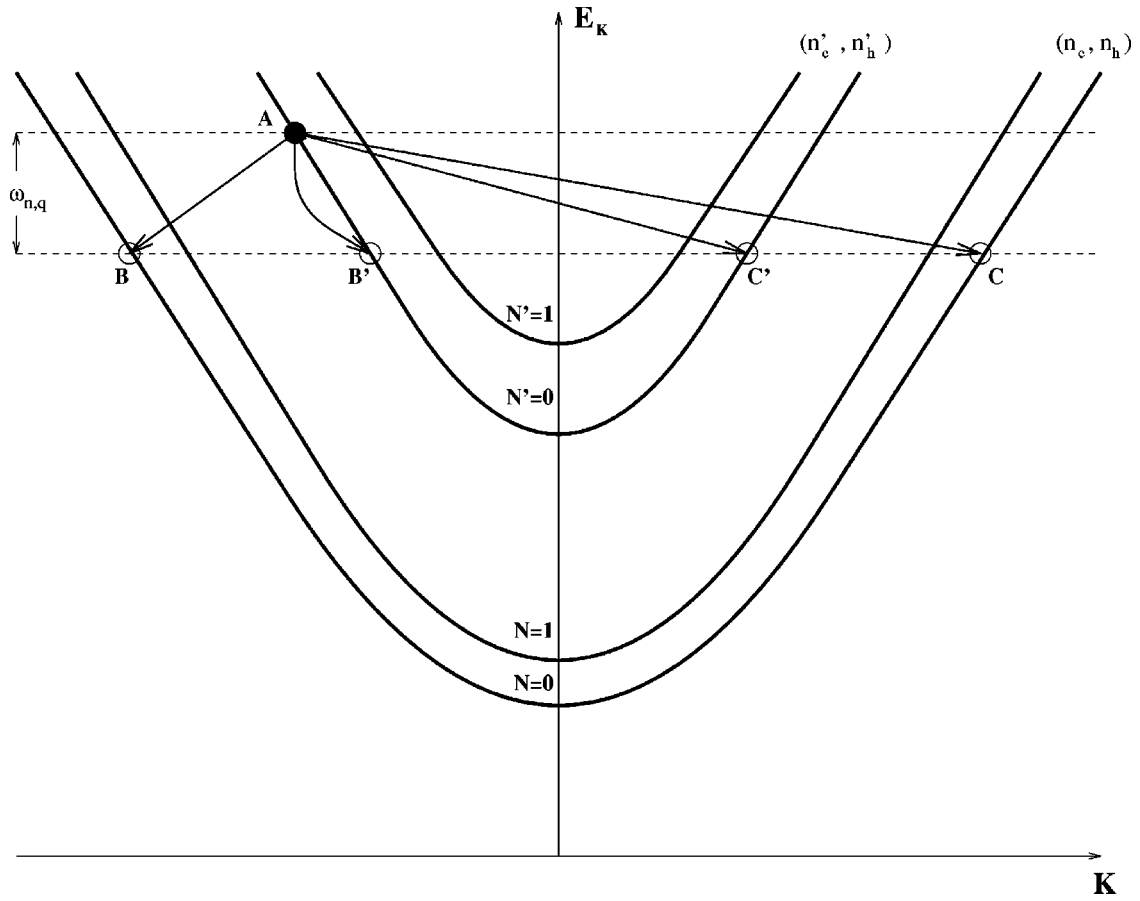

FIG. 4. Schematic representation of allowed scattering processes. See text, Sec. II, for discussion.

IV. DISCUSSION AND CONCLUSIONS

For the numerical calculations of the scattering rate we select the GaAs/AlAs parameters given in Table I. The hole effective masses are described by the Luttinger parameters, where the in plane hole masses are equal to $m_{\perp}^{h}=m_0/(\gamma_1 \pm \gamma_2)$ while along the Z direction $m_h^z=m_0/(\gamma_1 \mp 2\gamma_2)$.[24] The sign $+(-)$ corresponds to light (heavy) character of the mass along the Z direction (heavy or light character on the XY plane). In Fig. 5 we show the dependence of $W^{(n_p)}_{0;1,1\rightarrow 0;1,1}$ on E_K for the excitonic ground transition $N=0\rightarrow N=0$ and a QW width $d=4.2$ nm. In the inset the corresponding GaAs phonon dispersion is represented. The calculation presents the heavy- (solid lines) and light-hole (dashed lines) contribution along the quantum-well growth direction corresponding to the L_2, L_4, and L_8 phonon modes. Since we are dealing with intraband transitions ($n_e=n_h=1$ for the final and initial states) the exciton-phonon interaction with odd modes is forbidden and the main contribution correspond to the L_2 mode. In the figure it can be seen that L_4 is almost nine and two times weaker than L_2 and L_8 modes, respectively. To explain the above results we need to look back at the phonon dispersion in the inset of the figure. The L_2 and L_4 confined phonons are almost flat while the L_8 presents a stronger dispersion as a function of the phonon wave number **q** and it is, in addition, the symmetric QW phonon that has a predominantly interface character. The electrostatic potential associated to the L_8 mode gives strong exciton coupling by Fröhlich interaction in intrasubband transitions. The modes with largest $\varphi_{n_p,\mathbf{q}}$ component in Eq. (24) are those that have the largest interface contribution, explaining why the scattering rate associated to the L_8 mode in Fig. 5 is stronger that the L_4 confined phonon.

TABLE I. Parameters used in the present paper.

Parameters	GaAs	AlAs
E_g(eV)	1.5192[a]	3.1132[a]
ω_T (cm^{-1})	273.8[b]	
β_L	1.71[b]	
β_T	1.77[b]	
m_e/m_0	0.0665[a]	0.15[a]
γ_1	6.85[a]	3.45[a]
γ_2	2.10[a]	0.68[a]
ϵ_0	12.53[a]	10.06[a]
ϵ_0	10.983[a]	8.16[a]
ΔE_c(%)	65%	
ΔE_v(%)	35%	

[a]From Ref. 27.
[b]From Ref. 19.

Figure 6 shows the dependence of the total scattering probability $W^{(n_p)}_{0;1,1}(E_k) = \Sigma_{N'=0,1,2} W^{(n_p)}_{0;1,1\rightarrow N';1,1}(E_K)$ on E_k

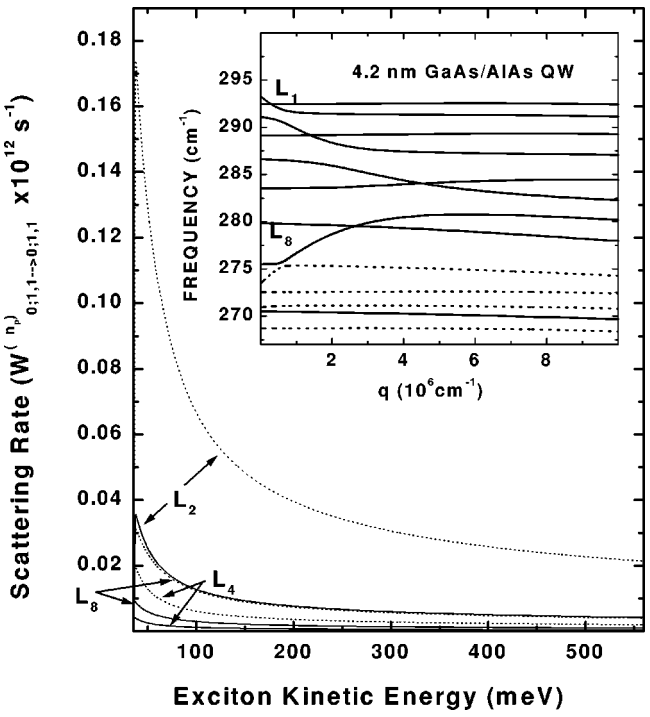

FIG. 5. One-phonon assisted exciton intrasubband scattering rate $W^{(n_p)}_{0;1,1\to0;1,1}$ in a GaAs/AlAs QW as a function of the in-plane center-of-mass exciton kinetic energy. Dashed lines (solid lines) correspond to the light-hole (heavy hole) mass along the QW growth direction with $d=4.2$ nm. The inset shows the GaAs phonon dispersion. The L_2, L_4, and L_8 phonon modes according to the notation followed in inset have been considered in the calculation.

and different quantum-well widths. Figure 6 (a) corresponds to a QW width $d=2.8$ nm while (b) and (c) to $d=2.0$ and 1.7 nm, respectively. In the calculation, we present the heavy hole (solid lines) and light hole (dashed lines) along the Z direction for $n_p=2$ and 4 and the two main peaks observed in the figures are due to $N=0\to N=0$ and $N=0\to N=1$ excitonic transitions. It can be seen that for $d=2.8$ nm the L_2 mode is almost two time stronger than the L_4 one, while the opposite is observed when the QW width is reduced to $d=2.0$ nm, that is the L_2 confined phonon contribution is weaker than the L_4 mode. For $d=1.7$ nm the exciton scattering rate due to $n_p=4$ is negligible [not shown in Fig. 6(c)] but T_1 becomes the stronger ones for $E_k>50$ meV. As in the case of Fig. 5, the phonon mode that has a predominantly interface character presents a strong coupling with excitons by the Fröhlich interaction via the largest electrostatic potential $\varphi_{n_p,\mathbf{q}}$. According to the phonon dispersions shown in Fig. 3. We see that the symmetric QW phonon are L_4 and T_1 for $d=2.0$, and 1.7 nm, respectively, explaining why the scattering rate assisted by the L_4 phonon in Fig. 6(b) and T_1 in Fig. 6(c) are stronger than or equal to that due to the L_2 confined mode. In the case of $d=1.7$ nm the L_4 phonon mode is more confined with an almost flat dispersion relation [see Fig. 3(c)]. For the range of q values where the phonons are flat the Fröhlich interaction is proportional to $1/\sqrt{q^2+q_z^2}$ with $q_z=n_p\pi/d$ ($n_p=1,2,\ldots$).[19] Hence, the contribution to the intraband scattering rate of the $n_p=4$ mode has to be almost four times weaker than for the $n_p=2$.

Let us comment on the effect of the carrier effective masses on the scattering rate. First, the confinement is a function of the hole masses along the Z axis; second, the hole-phonon matrix element depends on the hole masses through the $Q_h=m^h_\perp/Mqa_B$ factor and the range of values $q_{min}\leqslant q\leqslant q_{max}$ is a function of the in plane electron-hole mass; third, the scattering probability value strongly depends on the in-plane density of states. Fig. 6 shows that the total scattering probability $W^{(n_p)}_{0;1,1}(E_k)$ for the case of the light-hole mass along the Z direction (heavy-hole character in the XY plane) is stronger than the heavy-hole exciton one, and that the relative intensity between several phonon branches is only a function of the phonon dispersion which itself depends on the QW width. It is important to note that for the case we consider of isotropic effective masses and $m_e=m^h_\perp$ the intra-band transition $W^{(n_p)}_{0\to0}$ is identically zero.[2]

In conclusion, we have performed an analysis of the exciton scattering rate in narrow QWs. The relaxation of hot excitons accounts for the emission of confined and interface optical longitudinal phonons due to the Fröhlich-like exciton-phonon interaction. The results obtained show a different behavior of the scattering probability as a function of the well width and in-plane exciton kinetic energy. The value of $W^{(n_p)}_{0\to0}$ is not equal to zero for $E_K>\hbar\omega_{n_p,0}$ (for the case of intra-subband transition), increases with increasing E_K reaching a maximum, and begins to fall according to the law $E_K^{-1/2}$.[25] The relative strength of the different phonon modes is proportional to the ratio of the square of their overlap integral of the function $\varphi_{n_p,\mathbf{q}}$ with initial and final electron and hole subband states in the QW. The Fröhlich Hamiltonian (13) presents a definite parity, and the antisymmetric part of the potential $\varphi_{n_p,\mathbf{q}}(z)$ (L_1,L_3 modes) couples to the exciton in inter-subband transitions (in our case $n_h\neq n'_h$) with exciton wave functions having different symmetry with respect to the center of the well. For a given phonon state, inter-subband transitions are less efficient processes (in our calculation one order de magnitude smaller than the case of intra-band transition) on the exciton relaxation time in comparison with the intra-band probability. The intra-subband scattering rate is accompanied only by symmetric phonon states (L_2,$L_4\ldots$).

These results together with Eq. (1) predict that MPR spectra in the Γ-point have to be composed mostly by combinations of even modes in completely correspondence with Raman spectra shown in Fig. 1. For samples with 10-GaAs monolayer width combination such as $3L_2$, $2L_2+L_4$, and L_2+2L_4 are observed in the GaAs phonon spectra. In the case of the 6-GaAs monolayer well width, only the combination of L_2 and interface GaAs modes ($3L_2$, $2L_2+IF$, etc.) are reported. Spectra of Fig. 1 correspond to excitation energies above the type-I band gap of 125 and 122 meV for the (10,10) and (6,6) samples, respectively.[15] A theoretical estimation of the relative intensities for the even modes can be obtained from Eq. (1). Taking into account that the total exciton scattering rate, W_α, in a given state α is constant, the

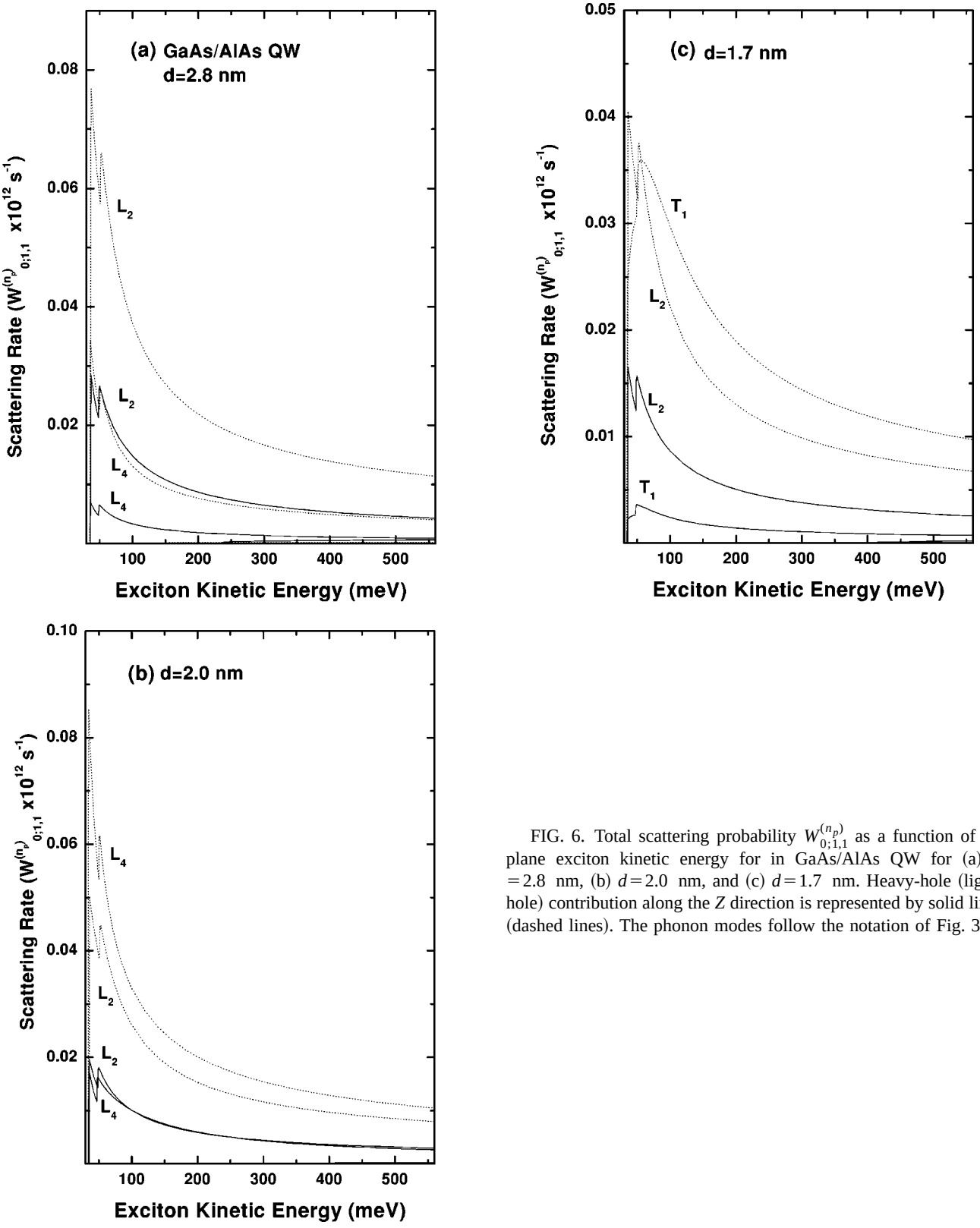

FIG. 6. Total scattering probability $W^{(n_p)}_{0;1,1}$ as a function of in-plane exciton kinetic energy for in GaAs/AlAs QW for (a) $d=2.8$ nm, (b) $d=2.0$ nm, and (c) $d=1.7$ nm. Heavy-hole (light-hole) contribution along the Z direction is represented by solid lines (dashed lines). The phonon modes follow the notation of Fig. 3.

relative intensities for $3L_2$, $L_2+L_4+L_2$, and L_2+IF+L_2 process are given by

$$\frac{I^{(3n_2)}}{I^{(n_2+n_4+n_2)}} \sim \frac{W^{(n_2)}_{0;1,1\to 0;1,1}(E_K)}{W^{(n_4)}_{0;1,1\to 0;1,1}(E_K)},$$

$$\frac{I^{(3n_2)}}{I^{(n_2+IF+n_2)}} \sim \frac{W^{(n_2)}_{0;1,1\to 0;1,1}(E_K)}{W^{IF}_{0;1,1\to 0;1,1}(E_K)}.$$

A direct evaluation of $W^{(n_2)}_{0;1,1\to 0;1,1}(E_K)/W^{(n_4)}_{0;1,1\to 0;1,1}(E_K)$ and taking into account the light-hole contribution for the 10 and

6-GaAs monolayers gives values of 2.7 and 117, respectively. That is, in a six monolayers sample, the MPR at the Γ point by combinations of L_2 and L_4 confined phonons must be almost forbidden. The opposite conclusion arises for $d=2.8$ nm case, when the combined intensities of L_2 and L_4 phonons are comparable to the intensity due to $3L_2$. We need to remark that for the $2L_2+L_4$ process we have three terms instead of one as in the case of $3L_2$ confined phonon and the total third-order Raman intensity of $I^{(2L_2+L_4)}\approx I^{(3L_2)}$. As we know from Figs. 3(a) and (c), the *IF* modes correspond to the T_1 hybrid mode. The relative intensity $I^{(3n_2)}/I^{(n_2+IF+n_2)}$ gives a value of 0.8 for the (6,6) samples. That is, the 6-GaAs monolayers favors the combination of L_2 with *IF* modes with a total intensity higher with respect to $3L_2$ phonon. These results are in complete agreement with the experimental observation of Fig. 1 explaining the observer variation of the MPR light scattering on the QW widths. Hence, the experimental observation in GaAs/AlAs superlattices on the relative intensities of multiphonon scattering can be explained in the framework of a MPR cascade model taking into account the relative role of the confined and interface phonons on the hot-exciton scattering rate and on the QW width. A more detailed theory on the present issue has to take into account the indirect creation and annihilation probability for the type-I GaAs exciton in terms of the phonon mode and QW parameters.

ACKNOWLEDGMENTS

This work was supported in part by a grant from the World Laboratory, Lausanne. Support is also acknowledged from the Science Division of the The City College of CUNY and from the CUNY-Caribbean Exchange Program.

APPENDIX

1. Exciton-phonon interaction

The norm of the vibrational amplitude is equal to

$$\|u\|^2=\int_{-d/2}^{d/2}[Y^2(z)+Z^2(z)]dz, \tag{A1}$$

where for odd-potential states

$$Y(z)=\eta_q\sin\left(\frac{2\eta_L z}{d}\right)-\eta_T\frac{S_L^-\exp(\eta_q)+S_L^+\exp(-\eta_q)}{C_T^-\exp(\eta_q)-C_T^+\exp(-\eta_q)}\sin\left(\frac{2\eta_T z}{d}\right)+S_L^+\frac{\omega_L^2-\omega_T^2}{\omega_L^2-\omega^2}\exp(-\eta_q)\sinh\left(\frac{2\eta_q z}{d}\right), \tag{A2}$$

$$Z(z)=\eta_L\cos\left(\frac{2\eta_L z}{d}\right)+\eta_q\frac{S_L^-\exp(\eta_q)+S_L^+\exp(-\eta_q)}{C_T^-\exp(\eta_q)-C_T^+\exp(-\eta_q)}\cos\left(\frac{2\eta_T z}{d}\right)+S_L^+\frac{\omega_L^2-\omega_T^2}{\omega_L^2-\omega^2}\exp(-\eta_q)\cosh\left(\frac{2\eta_q z}{d}\right), \tag{A3}$$

and for even states

$$Y(z)=\eta_q\cos\left(\frac{2\eta_L z}{d}\right)+\eta_T\frac{C_L^-\exp(\eta_q)-C_L^+\exp(-\eta_q)}{S_T^-\exp(\eta_q)+S_T^+\exp(-\eta_q)}\cos\left(\frac{2\eta_T z}{d}\right)+C_L^+\frac{\omega_L^2-\omega_T^2}{\omega_T^2-\omega^2}\exp(-\eta_q)\cosh\left(\frac{2\eta_q z}{d}\right), \tag{A4}$$

$$Z(z)=\eta_L\sin\left(\frac{2\eta_L z}{d}\right)-\eta_q\frac{C_L^-\exp(\eta_q)-C_L^+\exp(-\eta_q)}{S_T^-\exp(\eta_q)+S_T^+\exp(-\eta_q)}\sin\left(\frac{2\eta_T z}{d}\right)-C_L^+\frac{\omega_L^2-\omega_T^2}{\omega_T^2-\omega^2}\exp(-\eta_q)\sinh\left(\frac{2\eta_q z}{d}\right), \tag{A5}$$

where

$$S_{L(T)}^{\pm}=\sqrt{\eta_q^2+\eta_{L(T)}^2}\sin(\eta_{L(T)}\pm\theta_{L(T)}), \tag{A6}$$

$$C_{L(T)}^{\pm}=\sqrt{\eta_q^2+\eta_{L(T)}^2}\cos(\eta_{L(T)}\pm\theta_{L(T)}), \tag{A7}$$

$$S_0=\frac{S_L^- e^{\eta_q}+S_L^+ e^{-\eta_q}}{2\eta_q}, \tag{A8}$$

$$C_0=\frac{C_L^- e^{\eta_q}-C_L^+ e^{-\eta_q}}{2\eta_q}, \tag{A9}$$

and

$$\tan\theta_{L(T)}=\frac{\eta_{L(T)}}{\eta_q},\quad \eta_{L(T)}=\frac{d}{2}\sqrt{\frac{\omega_{L(T)}^2-\omega^2}{\beta_{L(T)}^2}-q^2},\quad \eta_q=\frac{dq}{2},$$

and ω_T is the TO bulk phonon frequency.

2. In-plane exciton-phonon matrix element

The matrix elements $I_{N,m}^{N',m'}$ represent the in-plane excitonic transitions. From Eq. (6) and Eq. (13) it follows that

$$I_{N,m}^{N',m'}=\langle N|\left(2(-1)^{|m'-m|}\times\int_0^{\pi}\cos(m'-m)\,\theta e^{im\rho q\cos\theta/M}d\theta\right)|N'\rangle, \tag{A10}$$

and θ being the angle between $\boldsymbol{\rho}$ and $\mathbf{q}$ vectors. The integration over θ gives

$$I_{N,m}^{N',m'}=(-i)^{|m'-m|}2\pi\langle N|J_{|m'-m|}\left(\frac{m}{M}\rho q\right)|N'\rangle, \tag{A11}$$

where $J_\nu(z)$ is the Bessel function of order ν. Substituting Eq. (7) into Eq. (A11), we have

$$I_{N,m}^{N',m'}=\lambda_N^2 a_B^2 N_{N,m}N_{N',m'}\frac{\lambda_N|m'|}{\lambda_{N'}}\times\int_0^{\infty}r^{|m|+|m'|+1}e^{-r(1+\lambda_N/\lambda_{N'})/2}\times F(-N+|m|,2|m|+1,r)\times F\left(-N'+|m'|,2|m'|+1,\frac{\lambda_N}{\lambda_{N'}}r\right)\times J_{|m'-m|}(Q\lambda_N r), \tag{A12}$$

with $\lambda_N=(N+1/2)/2$. The hypergeometric function $F(-N+|m|,2|m|+1,r)$ is a polynomial in r and the integral (A12) can be obtained making use of the identity[26]

$$\int_0^{\infty}x^{p+1}e^{-\alpha x}J_\nu(\beta x)dx=(-1)^{p+1}\beta^{-\nu}\frac{d^{p+1}}{d\alpha^{p+1}}\left[\frac{(\sqrt{\alpha^2+\beta^2}-\alpha)^\nu}{\sqrt{\alpha^2+\beta^2}}\right], \tag{A13}$$

with $\beta>0$ and $\nu>0$. We thus find

$I_{0,0}^{N,m}(Q)$	$m=0$	$m=\pm1$	$m=\pm2$
$N=0$	$\frac{1}{2\pi}\frac{1}{(1+Q^2)^{3/2}}$		
$N=1$	$\frac{1}{2\pi\sqrt{3^3}}\frac{Q^2}{(\frac{4}{9}+Q^2)^{5/2}}$	$\frac{-i\sqrt{2}}{6\pi\sqrt{3^3}}\frac{Q}{(\frac{4}{9}+Q^2)^{5/2}}$	
$N=2$	$\frac{1}{2\pi\sqrt{5^3}}\frac{2Q^2+\frac{9}{25}}{(Q^2+\frac{9}{25})^{7/2}}$	$\frac{-i}{2\pi\sqrt{5^3}}\frac{\sqrt{6}}{10}\frac{Q(2Q^2+\frac{9}{25})}{(Q^2+\frac{9}{25})^{7/2}}$	$\frac{-1}{2\pi\sqrt{5^3}}\frac{\sqrt{9}}{50\sqrt{6}}\frac{Q^2}{(Q^2+\frac{9}{25})^{7/2}}$

[1] E. Gross, S. Permogorov, Ya. Morozenko, and B. Kharlamov, Phys. Status Solidi B **59**, 551 (1973).

[2] K.A. Aristora, C. Trallero-Giner, I.G. Lang, and S.T. Pavlov, Phys. Status Solidi B **85**, 351 (1978).

[3] C. Trallero-Giner, I.G. Lang, and S.T. Pavlov, Fiz. Tekh. Poluprovodn. **14**, 235 (1980) [Sov. Phys. Semicond. **14**, 138 (1980)].

[4] C. Trallero-Giner, L.I. Korovin, and S.T. Pavlov, Fiz. Tverd. Tela **19**, 2456 (1977) [Sov. Phys. Solid State **19**, 1438 (1977)].

[5] V.F. Sapega, M.P. Chamberlain, T. Ruf, M. Cardona, D.N. Mirlin, K. Tötemeyer, A. Fisher, and K. Eberl, Phys. Rev. B **52**, 14 144 (1995).

[6] Jagdeep Shah, *Ultrafast Spectroscopy in Semiconductors and Semiconductor Nanostructures* (Springer-Verlag, Berlin, 1999).

[7] M.C. Thatan, J.F. Ryan, and C.T. Foxon, Phys. Lett. **63A**, 1637 (1989).

[8] K.T. Tsen, K.R. Wald, T. Ruf, P.Y. Yu, and H. Morkoc, Phys. Lett. **63**, 2557 (1991).

[9] S.-C. Lee, and I. Galbraith, Phys. Rev. B **59**, 15 796 (1999).

[10] H.N. Spector, J. Lee, and P. Melman, Phys. Rev. B **34**, 2554 (1986).

[11] S. Rudin and T.L. Reineke, Superlattices Microstruct. **3**, 137 (1987).

[12] S. Rudin, T.L. Reineke, and B. Segal, Phys. Rev. B **42**, 11 218 (1990).

[13] T. Hiroshima, Solid State Commun. **68**, 483 (1988).

[14] F. Clérot, B. Deveaud, A. Chomette, A. Regreny, and B. Sermage, Phys. Rev. B **41**, 5756 (1990).

[15] D.J. Mowbray, M. Cardona, and K. Ploog, Phys. Rev. B **43**, 11 815 (1991).

[16] E.L. Ivchenko, I.G. Lang, and S.T. Pavlov, Fiz. Tverd. Tela (Leningrad) **19**, 1227 (1977) [Sov. Phys. Solid State **19**, 718 (1977)].

[17] E. Menéndez-Proupin, C. Trallero-Giner, and S.E. Ulloa, Phys. Rev. B **60**, 16 747 (1999).

[18] M. Shinada and S. Sugono, J. Phys. Soc. Jpn. **21**, 1936 (1966).

[19] C. Trallero-Giner, R. Pérez-Alvarez, and F. García-Moliner, *Long Wave Polar Modes in Semiconductor Heterostructures*

(Pergamon/Elsevier Science, London, 1998).
[20] M. Zunke, R. Shorer, G. Abstreiter, W. Klein, G. Weimann, and M.P. Chamberlain, Solid State Commun. **93**, 847 (1995).
[21] A.J. Shields, M. Cardona, and K. Eberl, Phys. Rev. Lett. **72**, 412 (1994).
[22] C. Trallero-Giner, E. Menendez-Proupin, A. Debernardi, and M. Cardona, Phys. Rev. B **57**, 4664 (1998).
[23] F. Comas, R. Pérez-Alvarez, C. Trallero-Giner, and M. Cardona, Superlattices Microstruct. **14**, 95 (1993).
[24] A. Balderechi and O. Lipari, Phys. Rev. B **3**, 439 (1971).
[25] For the case of bulk semiconductors the asymptotic behavior of the scattering rate follows the same law as $1/\sqrt{E_K}$.[2]
[26] I.S. Gradshteyn and I.M. Ryzhik, *Tables of Integrals, Series and Products* (Academic, New York, 1980).
[27] *Landolt-Börstein Tables*, edited by O. Madelung, H. Shultz, and H. Weiss (Springer, Berlin, 1982), Vol. III/17a and 22a.